

Novel sphene coatings on Ti–6Al–4V for orthopedic implants using sol–gel method

Chengtie Wu^a, Yogambha Ramaswamy^a, David Gale^a, Wenrong Yang^b, Keqin Xiao^c,
Liangchi Zhang^c, Yongbai Yin^b, Hala Zreiqat^{a,*}

^a *Biomaterials and Tissue Engineering Research Unit, Biomedical Engineering, School of AMME, The University of Sydney, Sydney, 2006 NSW, Australia*

^b *EMU, The University of Sydney, Sydney, 2006 NSW, Australia*

^c *Mechanical Engineering, School of AMME, The University of Sydney, Sydney, 2006 NSW, Australia*

Received 22 September 2007; received in revised form 29 October 2007; accepted 19 November 2007

Available online 24 November 2007

Abstract

Hydroxyapatite (HAp) is commonly used to coat titanium alloys (Ti–6Al–4V) for orthopedic implants. However, their poor adhesion strength and insufficient long-term stability limit their application. Novel sphene (CaTiSiO₅) ceramics possess excellent chemical stability and cytocompatibility. The aim of this study is to use the novel sphene ceramics as coatings for Ti–6Al–4V. The sol–gel method was used to produce the coatings and the thermal properties, phase composition, microstructure, thickness, surface roughness and adhesion strength of sphene coatings were analyzed by differential thermal analysis–thermal gravity (DTA–TG), X-ray diffraction (XRD), scanning electron microscopy (SEM), atom force microscopy (AFM) and scratch test, respectively. DTA analysis confirmed that the temperature of the sphene phase formation is 875 °C and XRD analysis indicated pure sphene coatings were obtained. A uniform structure of the sphene coating was found across the Ti–6Al–4V surface, with a thickness and surface roughness of the coating of about 0.5–1 μm and 0.38 μm, respectively. Sphene-coated Ti–6Al–4V possessed a significantly improved adhesion strength compared to that for HAp coating and their chemical stability was evaluated by testing the profile element distribution and the dissolution kinetics of calcium (Ca) ions after soaking the sphene-coated Ti–6Al–4V in Tris–HCl solution. Sphene coatings had a significantly improved chemical stability compared to the HAp coatings. A layer of apatite formed on the sphene-coated Ti–6Al–4V after they were soaked in simulated body fluids (SBF). Our results indicate that sol–gel coating of novel sphene onto Ti–6Al–4V possessed improved adhesion strength and chemical stability, compared to HAp-coated Ti–6Al–4V prepared under the same conditions, suggesting their potential application as coatings for orthopedic implants.

© 2007 Acta Materialia Inc. Published by Elsevier Ltd. All rights reserved.

Keywords: Sphene; Orthopedic; Titanium alloy; Surface chemistry modification

1. Introduction

The success of orthopedic implants depends on strong anchorage of the device to skeletal tissue. Titanium alloys (Ti–6Al–4V) are widely used as orthopedic and dental implant materials due to its excellent biocompatibility including low toxicity, great stability with low corrosion rates and favorable mechanical properties compared to

other metals [1,2]. However, the host response to Ti–6Al–4V is not always favorable and a fibrous layer may form at the skeletal tissue/device interface causing aseptic loosening of the device. Hence, there is a need to develop new engineered surfaces to provide better biological outcomes. Various surface modifications have been applied to Ti–6Al–4V in an attempt to enhance bone differentiation and promote direct contact between bone and implant material. One such approach is coating Ti–6Al–4V with bioactive ceramics such as HAp and CaSiO₃ [3–6]. However, the major drawback of the HAp coatings is that they cannot maintain long-term stability, and in certain situations

* Corresponding author. Tel.: +61 2 93512392; fax: +61 2 93517060.

E-mail address: hzeiqat@usyd.edu.au (H. Zreiqat).

delamination of the HAp coatings from the alloy occurs due to their poor bond strength and insufficient chemical stability [7–9]. Although CaSiO₃ coatings produced good bioactivity and enhanced short-term osseointegration properties of the implant [5], their poor chemical stability remains to be a major drawback and their long-term stability is questionable [10–12]. Therefore, the aim of this study is to develop novel bioactive coatings for use onto Ti–6Al–4V to address the drawbacks of the currently used coating materials.

Recently, we developed novel modified calcium silicate material, sphene (CaTiSiO₅) ceramics, which possess excellent chemical stability [13]. The thermal expansion coefficient of Ti–6Al–4V ($(8.4\text{--}8.8) \times 10^{-6} \text{ K}^{-1}$) is similar to that of sphene ($6 \times 10^{-6} \text{ K}^{-1}$). Therefore heat-treatment can be used to increase the crystallinity, reduce the residual stresses and enhance mechanical properties without creating tension between the coating and the underlying titanium substrate. In addition, sphene was found to support primary human osteoblastic-like cells (HOBs) attachment, proliferation and differentiation, indicating their excellent cytocompatibility [13]. The aim of this study is to use the novel sphene to coat Ti–6Al–4V, thereby producing an alloy with a coated material that has improved adhesion strength and chemical stability.

2. Materials and methods

2.1. Preparation of coatings

Sphene coating on Ti–6Al–4V disks were prepared by the sol–gel spinning method using tetraethyl orthosilicate ((C₂H₅O)₄Si, TEOS, Sigma–Aldrich, USA), titanium (IV) butoxide (Ti(O(CH₂)₃CH₃)₄, Ti(Bu)₄, Sigma–Aldrich, USA) and calcium nitrate tetrahydrate (Ca(NO₃)₂ · 4H₂O, Sigma–Aldrich, USA) as raw materials. Briefly, TEOS and Ti(Bu)₄ were mixed with ethanol and 2 M HNO₃ (mol. ratio: TEOS/Ti(Bu)₄/ethanol/HNO₃ = 1:1:10:0.08) and hydrolyzed for 30 min while stirring. HNO₃ is used to catalyze the hydrolysis of TEOS. The Ca(NO₃)₂ · 4H₂O were added into the mixture (mol. ratio: TEOS/Ti(Bu)₄/Ca(NO₃)₂ · 4H₂O = 1:1:1), and reactants were stirred for 5 h, then aged for 1 day at room temperature for coating. For evaluation of thermal behavior of sphene, dry gel of the sphene was prepared using the same method above and characterized by differential thermal analysis–thermal gravity (DTA–TG, Shimadzu Analyzer) from room temperature to 1100 °C.

Ti–6Al–4V disks (Biology Bridge Co., China) with a roughness of 100 nm were cleaned in water, followed by drying in acetone and ethanol for 10 min. Dried Ti–6Al–4V disks were fixed on the spinning machine with a controllable spinning speed and sphene sol solution was dropped to the substrate and spin-coated at 2000 rpm for 10 s. After drying at 60 °C for 24 h, samples were heated at 875 °C for 10 min in air with a heating rate of 4 °C min⁻¹. HAp sol–gel coated Ti–6Al–4V disks [14,15] were used as the control.

2.2. Characterization of coatings

The phase composition of the sphene powders and coatings was analyzed using X-ray diffraction (XRD, Siemens D5000, Germany) with a step size of 0.02° at a scanning rate of 1.2° min⁻¹. Surface morphology, composition and roughness of the Ti–6Al–4V-coated disks were analyzed by scanning electron microscopy (SEM, Philips XL 30 CP, The Netherlands) coupled with energy-dispersive spectrometer (EDS, Philips XL 30 CP, The Netherlands) and atomic force microscopy (AFM, Tempe, USA) with a tapping mode. For evaluation of the coating thickness, the coated disks were fixed in poly-methylmethacrylate (PMMA) and sections were cut using a diamond saw (Exakt 300CL; Exakt Apparatebau, Germany) and subsequently ground and polished with an Exakt 400 CS Micro Grinding System (Exakt Apparatebau, Germany) before analyzing using SEM.

2.3. Adhesion strength test

Scratch test was performed to quantify the adhesion strength of the coatings on Ti–6Al–4V disks. A constant load was applied on a diamond tip (84 μm in radius) to draw a line on the coatings. Optical microscopy was utilized to monitor any local and global failures. Different loads were used to draw lines to find the critical strength of the coating failure and the lines of critical failure were analyzed by SEM. The adhesion strength was calculated using the Hertz equations: $P_o = (P'E/\pi R)^{1/2}$, where P' is the load, R is the radius of diamond tip and E is the weighted E -modulus for the substrate material and diamond tip. E was calculated using the following equations:

$$1/E = [(1 - v_{\text{sub}}^2)/E_{\text{sub}}] + [(1 - v_{\text{tip}}^2)/E_{\text{tip}}]$$

where v_{sub} , E_{sub} , v_{tip} and E_{tip} are the Poisson ratios and E -moduli of substrate and diamond tip (see Table 1).

2.4. Chemical stability in Tris–HCl solution

For evaluation of the chemical stability of the coatings, the coated disks were soaked in the buffer solution of tris-(hydroxymethyl)-aminomethane (Tris, (CH₂OH)₃CNH₂) and hydrochloric acid (HCl) with a pH value of 7.4 for 1, 3 and 7 days, and the ratio of disk surface area to solution volume of Tris–HCl was 0.1 cm² ml⁻¹. After soaking, the disks were dried at 100 °C for 1 day. The samples before and after soaking were analyzed by second neutral mass spectrum (SNMS, INA-X, Specs GmbH, Germany)

Table 1
Mechanical properties of substrates and diamond tip

Materials	E -modulus (GPa)	Poisson ratio
Ti–6Al–4V	110	0.32
Diamond	1200	0.20

to evaluate the profile element change. The change of ion concentrations in Tris–HCl solution was analyzed by inductively coupled plasma atomic emission spectroscopy (ICP-AES; Perkin–Elmer, Optima 3000DV, USA) and the dissolution kinetic was calculated according to the released ion concentrations.

2.5. Apatite formation ability in SBF solution

Simulated body fluids (SBF) containing ion concentrations similar to those in human blood plasma were prepared as previously published [16,17]. Briefly, reagent-grade CaCl₂, K₂HPO₄ · 3H₂O, NaCl, KCl, MgCl₂ · 6H₂O, NaHCO₃ and Na₂SO₄ were dissolved in distilled water and pH adjusted to 7.4 with Tris and HCl. Sphene-coated disks were soaked in SBF at 37 °C for 21 day, and the ratio of disk surface area to solution volume of SBF was 0.1 cm² ml⁻¹. After soaking, the disks were dried at 100 °C for 1 day and coated with carbon before using SEM and EDS.

3. Results

3.1. Characterization of coatings

The DTA–TG curve of sphene dry gel is shown in Fig. 1. DTA analysis shows three endothermic peaks were observed at 122 °C, 508 °C and 560 °C, where weight loss was evident. At the higher temperature of 875 °C, the DTA curve shows a sharp exothermic peak and no weight loss was observed.

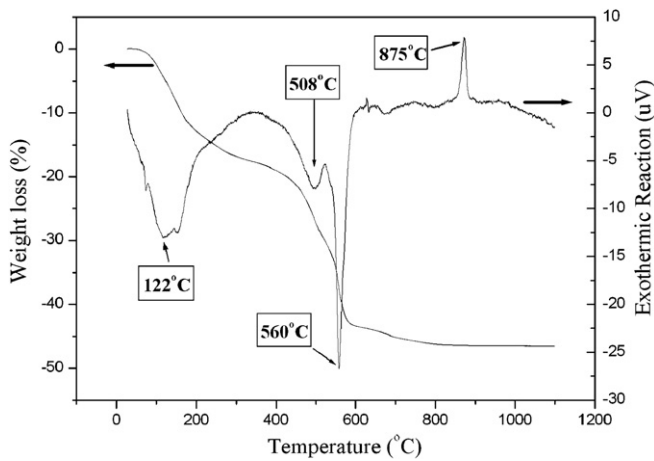


Fig. 1. DTA–TG analysis of sphene powders from room temperature to 1100 °C.

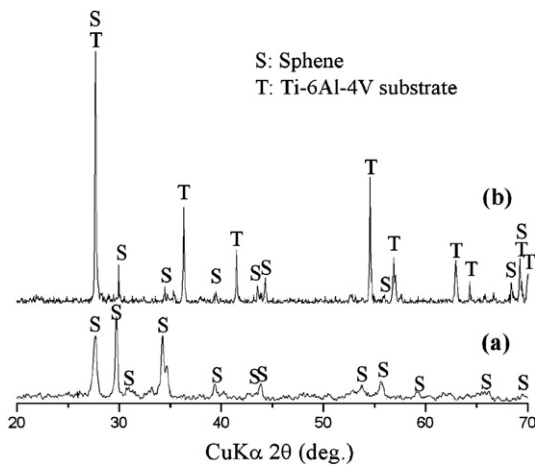


Fig. 2. XRD analysis of sphene powders (a) and coatings (b) sintering at same condition.

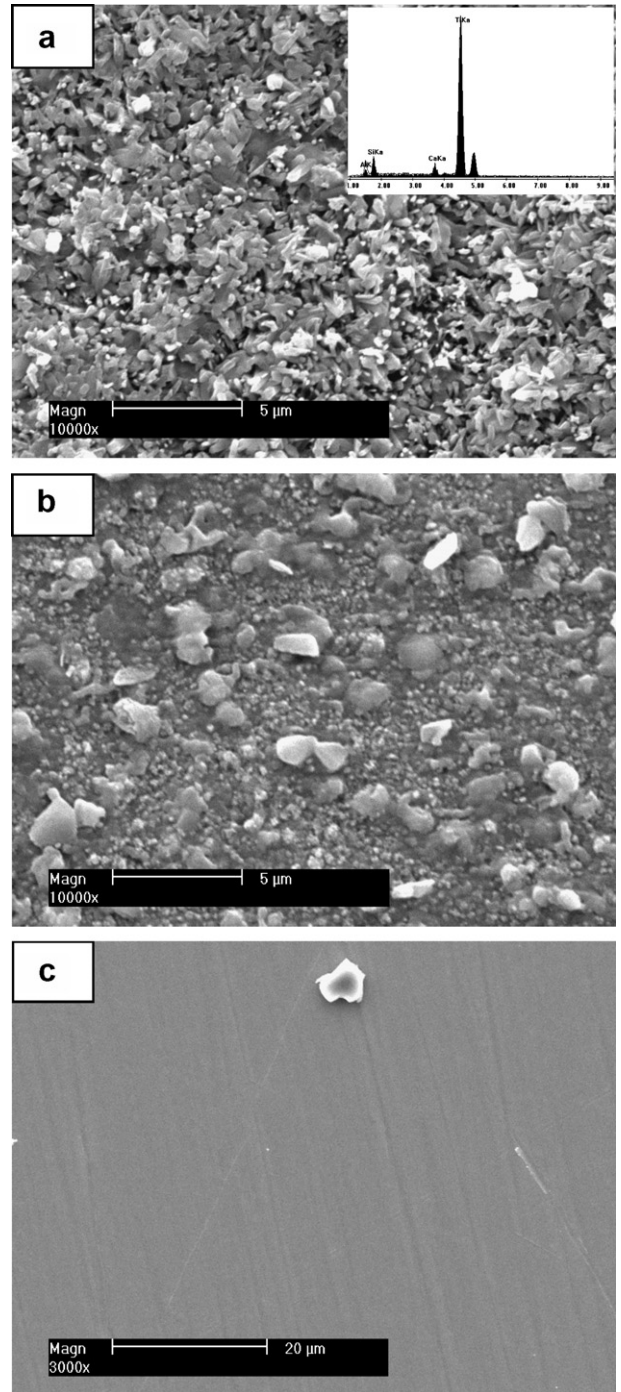


Fig. 3. SEM morphology and EDS analysis of sphene coating (a); HAP coating (b); Ti–6Al–4V substrates (c).

XRD analysis shows that only sphenes characteristic peaks exist in the pattern of sol-gel derived powders calcined at 875 °C (Fig. 2a) (Standard card no.: JCPD 11-0142). Besides the sphenes peaks in the coatings, there were diffraction peaks of Ti-6Al-4V substrates (Fig. 2b) as expected. Ti-6Al-4V surface is smooth (Fig. 3c) and the sphenes-coated Ti-6Al-4V produced uniform sphenes microcrystals with a size of about 200–500 nm (Fig. 3a) and possess a uniform thickness (about 0.5–1 μm) (Fig. 4). Ca, Si and Ti elements were evident in the sphenes coatings as indicated by the EDS analysis (Fig. 3a). HAp microcrystals cover the surface of Ti-6Al-4V substrates after sol-gel coatings (Fig. 3b). AFM analysis revealed that sphenes-coated Ti-6Al-4V possesses a comparable surface roughness ($0.38 \pm 0.04 \mu\text{m}$) with that of HAp coatings ($0.42 \pm 0.02 \mu\text{m}$), and both were significantly higher than that for the uncoated Ti-6Al-4V disks ($0.10 \mu\text{m}$) (Fig. 5).

3.2. Adhesion strength

The adhesion strength of the sphenes and HAp coatings on Ti-6Al-4V disks is shown in Table 2 and Fig. 6. At a load of 65 gram force (g.f.), the sphenes coating maintained its integrity and only minimal scratch existed on the surface of coating (Fig. 6a), compared to failure and damage of the HAp coating on Ti-6Al-4V when only 20 g.f. load was applied (Fig. 6d). At 25 g.f., the HAp coating was completely damaged and delamination occurred (Fig. 6e and f). In contrast, at a much higher load of 75 g.f., only minor damage was found on the sphenes coating (Fig. 6b arrow) and it was not until a load of 80 g.f. that most of the sphenes coatings failed and were damaged (Fig. 6c). The Hertz stress of coatings for sphenes is 17.4 MPa, indicating an improved bonding strength compared to that of HAp (9.8 MPa) (Table 2).

3.3. Chemical stability

In-depth elemental distribution profiles of sphenes and HAp coatings before and after 7 days of soaking in Tris-

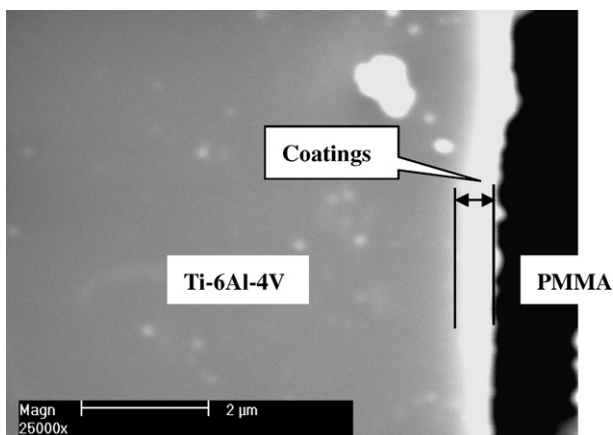


Fig. 4. SEM cross-section of sphenes coatings. The thickness is about 0.5–1 μm.

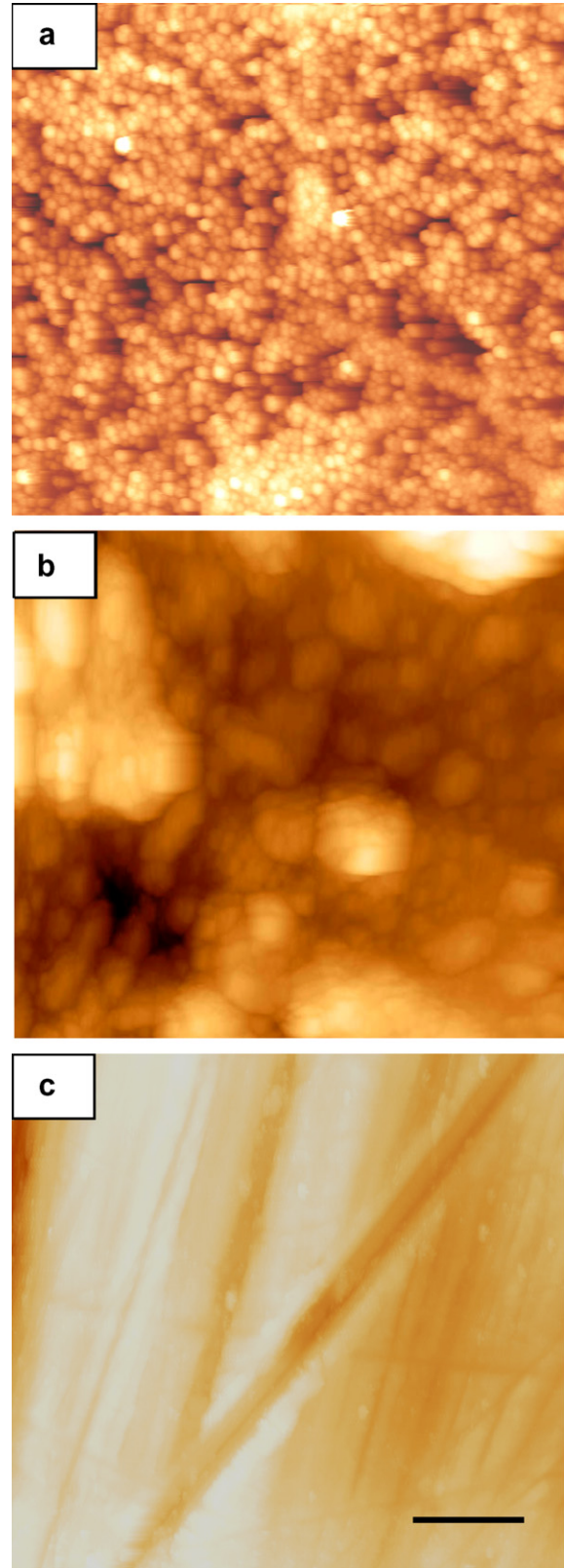


Fig. 5. AFM analysis of the average surface roughness: (a) sphenes coatings ($0.38 \pm 0.04 \mu\text{m}$); (b) HA coatings ($0.42 \pm 0.02 \mu\text{m}$); (c) Ti-6Al-4V substrates ($0.10 \pm 0.01 \mu\text{m}$). Data bar: 10 μm.

HCl solution were analyzed by SNMS (Fig. 7). After soaking, the intensity of silicon (Si) and Ca in the sphenes coating

Table 2
Hertz stress of coatings on Ti–6Al–4V substrates

Materials	Sphene	HAp
Hertz stress (MPa)	17.4 ± 0.9	9.8 ± 0.6

decreased from 28 to 25.6 CPS and 25 to 23 CPS, respectively (Fig. 7a and b), and the decrease rate is about 8.6% for Si and 8% for Ca. However, Ca and P in the HAp coating show a higher decrease rate of about 13% for Ca (from 15 to 13 CPS) and 25% for P (from 6 to 4.5 CPS) after soaking.

ICP-AES analysis of Ca dissolution kinetics of sphene and HAp coatings in Tris–HCl solutions are shown in Fig. 8. Sphene coatings possess a lower dissolution kinetics (0.00025) compared with that of HAp coating (0.00138).

3.4. Apatite formation ability in SBF

SEM and EDS analysis of the sphene coating soaked in SBF for 21 days are shown in Fig. 9. Some white particles are formed on the surface of the coating (Fig. 9a) which at higher magnification is found to be composed of lath-like nanocrystals (Fig. 9b). EDS analysis shows that the nanocrystals are apatite and the ratio of Ca/P is about 1.55 (Fig. 9c).

4. Discussion

During the last two decades, the use of bioactive materials that enhance bone apposition to hip joint prosthesis and dental screws has had considerable attention. HAp-coated orthopedic and dental implants have been widely tested but clinical trials indicate poor long-term implant survival and mechanical limitations in these applications [18,19]. Delamination of HAp coatings from Ti alloys occurs due to their poor bond strength and insufficient chemical stability [7–9]. More recently CaSiO_3 coatings produced good bioactivity and enhanced short-term osseointegration properties when coated onto Ti–6Al–4V implant [5]; however, their poor chemical stability and in turn long-term stability of the coated implants is questionable [10–12]. The present study demonstrates the development of a novel chemically stable sphene coating with enhanced bonding strength and chemical stability, compared to currently used HAp coatings, rendering it a suitable material for coating onto commonly used orthopedic and dental implants.

Sol–gel method was selected as our choice of coating technique as it has many advantages over the conventional plasma-spraying methods. Sol–gel method is performed at lower processing temperature [14,20] and can produce nano-sized particles or coatings which are extremely reactive when fired to moderately high temperatures, as well as producing coatings of higher purity and homogeneity [21]. Sol–gel method has a lower processing cost and the sol–

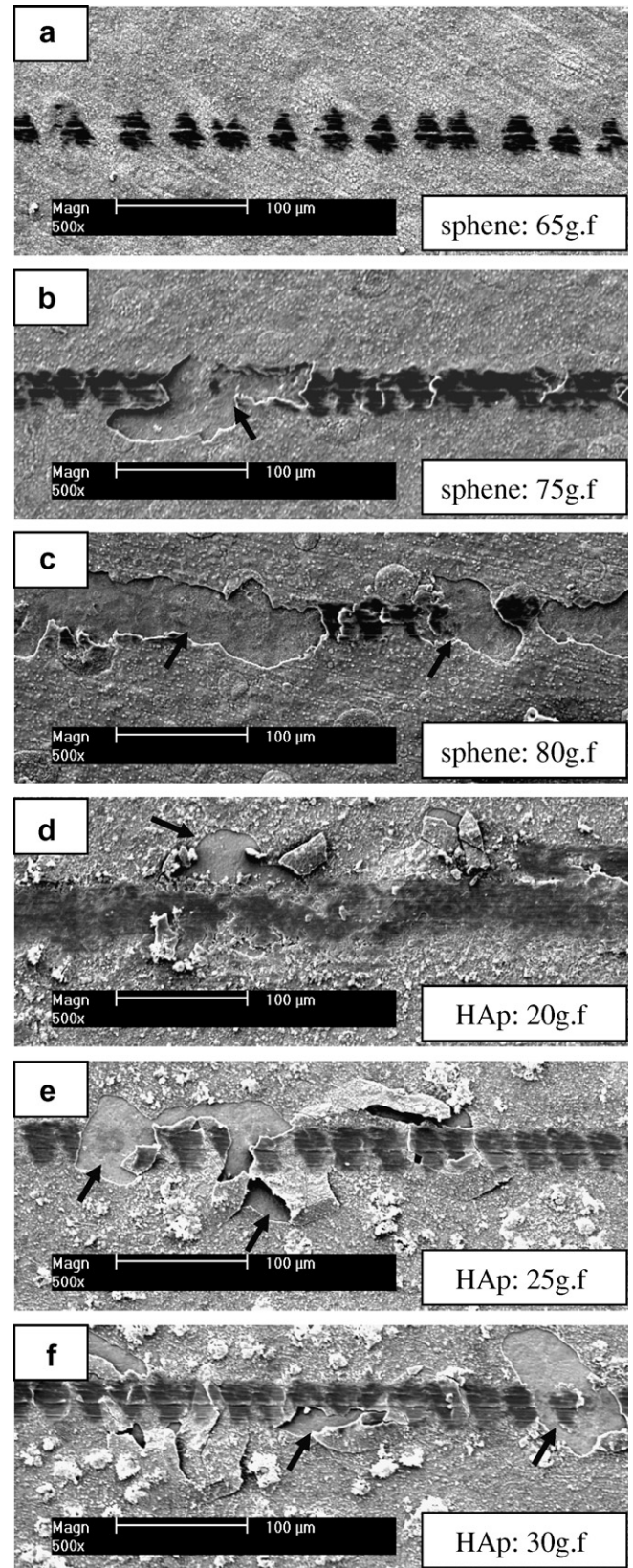


Fig. 6. The morphology of coatings after scratch test with different load. The arrows: coating failure. The corresponding Hertz stress is listed in Table 2.

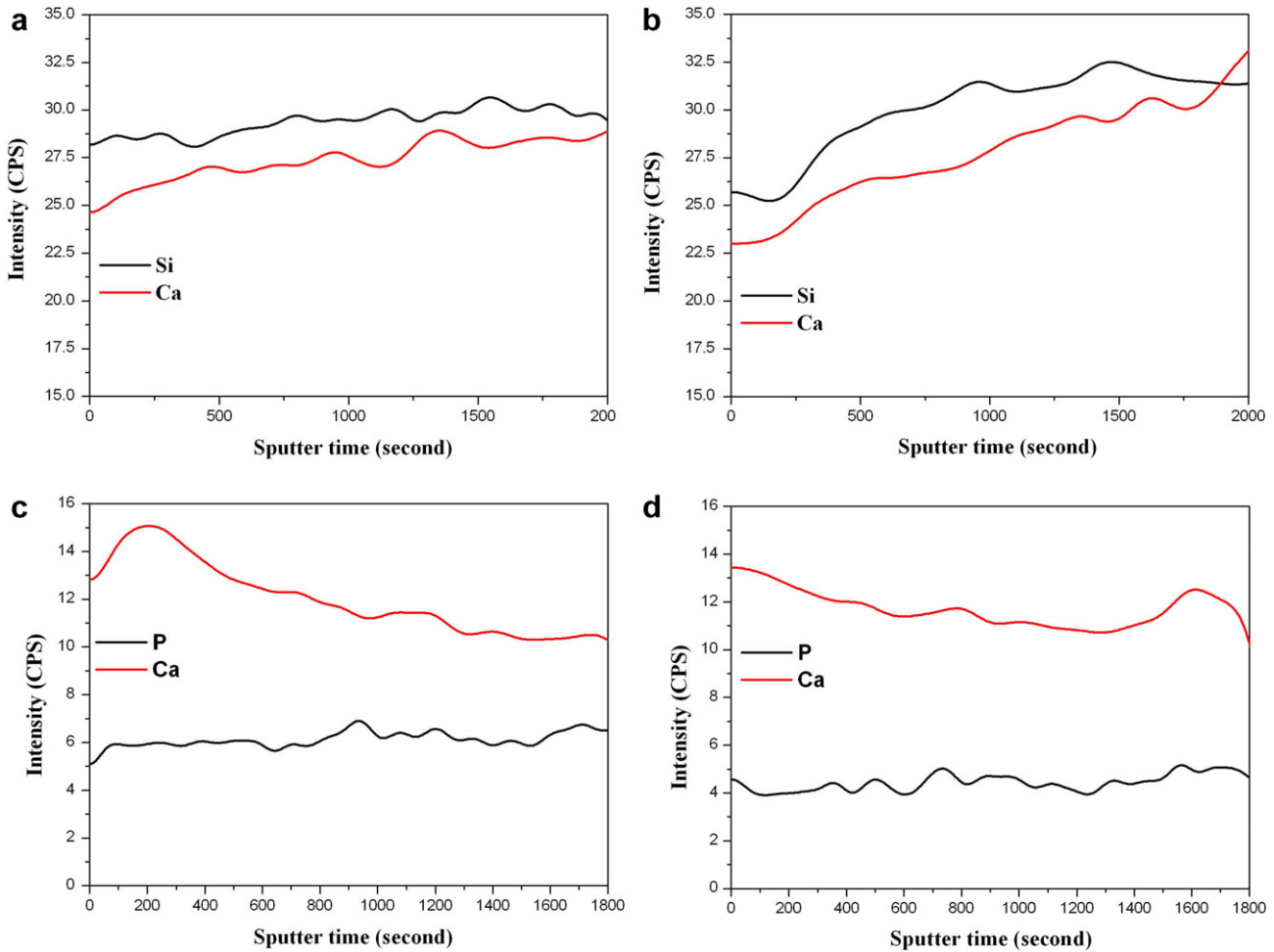


Fig. 7. In-depth element distribution profiles of sphene and HAp coating before and after 7 days of soaking in Tris-HCl solution by SNMS analysis: sphene before (a) and after (b) soaking; HAp before (c) and after (d) soaking.

gel route can be used for both coating and powder production. In this study, sphene coatings and powders were obtained by sol-gel method at the same sintering condition.

The thermal property of the gel is important to set the temperature of the phase transition of sphene when sinter-

ing the coating material. DTA-TG analysis indicates that the formation temperature for sphene phase is 875 °C as indicated in the sharp exothermic peak and maintenance of the weight of the powders. Three endothermic peaks were also evident at 122, 508 and 560 °C; this could be due to the evolution of alcohol and water in the gel, removal of structural water and decomposing of nitrate [22]. Sintering at 875 °C resulted in pure sphene crystal phase for both the powders and the final coating and SEM, EDS and AFM analysis confirmed the uniformity of the sphene coating.

Under controlled load and speed scratch test, performed by scratching the coated surface with a specified indenter [23,24], a higher load range of failure (65–80 g.f.) for sphene coatings was necessary to damage them compared to a much lower load range (20–30 g.f.) that caused the damage for HAp, indicating that sphene coating possesses an improved adhesion strength. Previous studies showed that the coating thickness affected the adhesion strength [7,25] of the coating to the underlying substrata. In the present study, the thickness of sphene coatings is about 0.5–1 μm, which is comparable to that previously found for HAp [14]. Therefore, the improved adhesion strength

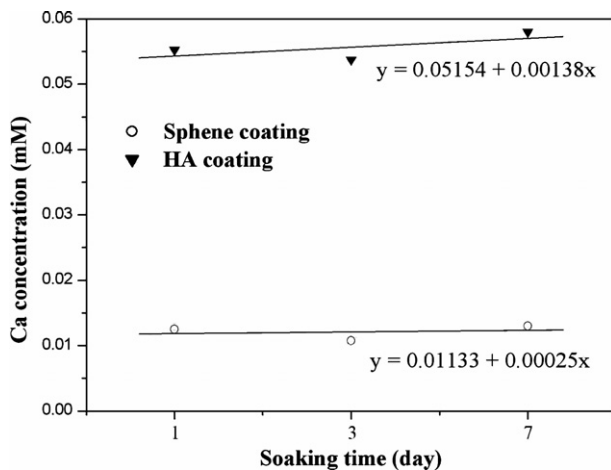


Fig. 8. Ca dissolution kinetics of sphene and HAp coatings after 1, 3 and 7 days soaking in Tris-HCl solution by ICP-AES analysis.

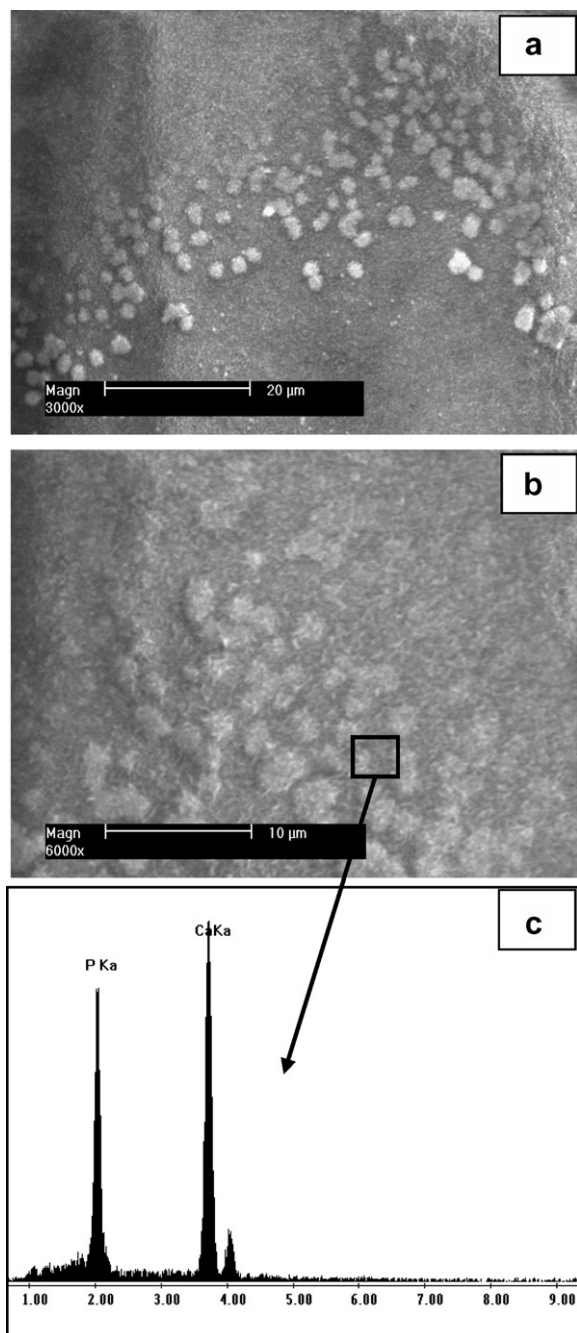


Fig. 9. SEM (a) and (b), and EDS (c) of sphene in SBF 21 days in simulated body fluids. The ratio of Ca/P = 1.55.

noted for the sphene coating cannot be attributed to the thickness of the coating, but rather to the intrinsic properties of the sphene. HAp possess a higher thermal expansion coefficient ($13.3 \times 10^{-6} \text{ K}^{-1}$) than that of Ti-6Al-4V ($(8.4-8.8) \times 10^{-6} \text{ K}^{-1}$), which will result in high residual stress and decrease the adhesion strength to the underlying substrata [8]. In contrast, sphene possesses a similar thermal expansion coefficient ($6 \times 10^{-6} \text{ K}^{-1}$) to Ti-6Al-4V, therefore, favoring their higher adhesion strength.

Chemical stability of the coating materials is another contributing factor to the long-term stability of the coatings [8,26]. In the present study, the chemical stability of

the sphene and HAp coatings was compared by testing the elemental profile and the dissolution kinetics of Ca ions after soaking the sphene and HAp-coated Ti-6Al-4V in Tris-HCl. Tris-HCl buffer was selected as it does not contain other foreign ions, such as Ca, Si and P. Our results show that the release of Ca (8%) and Si (8.6%) element from the sphene coatings is less than that for Ca (13%) and P (25%) elements released from the HAp coatings. Furthermore, the dissolution kinetics of Ca ions from the sphene coatings is lower than that of HAp coatings, indicating that sphene coatings possess an improved chemical stability, compared with HAp coatings.

Others have shown that a significant characteristic of bioactive materials is their ability to bond with living bone through the formation of an apatite layer on their surface both in vitro and in vivo [5,27,28]. Sphene coatings possess apatite formation ability in SBF, one of the measures for reflecting their bioactivity. Previous studies have shown that there are two mechanisms of apatite formation on bioactive materials after soaking in SBF. One is the release of some ions from the bioactive materials to form negative charge on the surface which will induce apatite formation [28,29]. The other is that specific microstructure with micro- and nanometer scale can provide the nucleation site for apatite formation [30,31]. Vayssieres et al. suggested that finer nano- or micro-crystalline particles possess higher surface charge densities than larger ones [32]. Small particles with increased molar free energy are more likely to absorb molecules or ions onto their surfaces in order to decrease the total free energy and to become more stable [30]. The sphene coating used in the present study represents a stable material with minimal release of ions from the material that may lead to the formation of negative surface charge. However, the formation of the apatite layer on the sphene coatings can be attributed to its microcrystallinity as being the key factor to induce apatite formation after soaking in SBF.

5. Conclusions

Sphene-coated Ti-6Al-4V disks have been successfully prepared by sol-gel spinning method. Characterizing the sphene coatings demonstrates that they are composed of microcrystals with uniform structure. The thickness and surface roughness of the coatings are in the range of 0.5–1 μm and 0.38 μm , respectively. Sphene coatings possess a significantly improved adhesion strength and chemical stability compared to HAp-coated Ti-6Al-4V. In addition, sphene coatings have the ability to form an apatite layer in SBF. Our results indicate the potential use of sphene coating materials for orthopedic and dental implants.

Acknowledgments

The authors would like to acknowledge the Australia National Health and Medical Research Council, the Australian Research Council, the University of Sydney

for providing a Postdoctoral Research Fellowship (Dr. Wu), and the technical support of Philip Boughton in using the spinning instruments for coatings. We acknowledge Dr. Peter Evans from ANSTO for performing the DTA measurements.

References

- [1] Okazaki Y, Rao S, Ito Y, Tateishi T. Corrosion resistance, mechanical properties, corrosion fatigue strength and cytocompatibility of new Ti alloys without Al and V. *Biomaterials* 1998;19(13):1197–215.
- [2] Okazaki Y, Gotoh E. Comparison of metal release from various metallic biomaterials in vitro. *Biomaterials* 2005;26(1):11–21.
- [3] Harle J, Kim HW, Mordan N, Knowles JC, Salih V. Initial responses of human osteoblasts to sol–gel modified titanium with hydroxyapatite and titania composition. *Acta Biomater* 2006;2(5):547–56.
- [4] Balani K, Chen Y, Harimkar SP, Dahotre NB, Agarwal A. Tribological behavior of plasma-sprayed carbon nanotube-reinforced hydroxyapatite coating in physiological solution. *Acta Biomater* 2007;3(6):944–51.
- [5] Xue W, Liu X, Zheng X, Ding C. In vivo evaluation of plasma-sprayed wollastonite coating. *Biomaterials* 2005;26(17):3455–60.
- [6] Liu X, Ding C, Wang Z. Apatite formed on the surface of plasma-sprayed wollastonite coating immersed in simulated body fluid. *Biomaterials* 2001;22(14):2007–12.
- [7] Kweh SW, Khor KA, Cheang P. An in vitro investigation of plasma sprayed hydroxyapatite (HA) coatings produced with flame-spheroidized feedstock. *Biomaterials* 2002;23(3):775–85.
- [8] Liu X, Chu P, Ding CX. Surface modification of titanium, titanium alloys, and related materials for biomedical application. *Mater Sci Eng R* 2004;47:49–121.
- [9] Bauer TW, Geesink RC, Zimmerman R, McMahon JT. Hydroxyapatite-coated femoral stems. Histological analysis of components retrieved at autopsy. *J Bone Joint Surg Am* 1991;73(10):1439–52.
- [10] Liu X, Ding C. Plasma sprayed wollastonite/TiO₂ composite coatings on titanium alloys. *Biomaterials* 2002;23(20):4065–77.
- [11] Wu CT, Ramaswamy Y, Kwik D, Zreiqat H. The effect of strontium incorporation into CaSiO₃ ceramics on their physical and biological properties. *Biomaterials* 2007;28:3171–81.
- [12] Liu X, Ding C. Plasma-sprayed wollastonite 2 M/ZrO₂ composite coating. *Surf Coat Tech* 2003;172(2–3):270–8.
- [13] Wu C, Ramaswamy Y, Soeparto A, Zreiqat H. Incorporation of titanium into calcium silicate improved their chemical stability and biological properties. *J Biomed Mater Res A*, in press.
- [14] Kim HW, Kim HE. Improvement of hydroxyapatite sol–gel coating on titanium with ammonium hydroxide addition. *J Am Ceram Soc* 2005;88(1):154–9.
- [15] Kim HW, Knowles JC, Salih V, Kim HE. Hydroxyapatite and fluor-hydroxyapatite layered film on titanium processed by a sol–gel route for hard-tissue implants. *J Biomed Mater Res B Appl Biomater* 2004;71(1):66–76.
- [16] Wu C, Ramaswamy Y, Boughton P, Zreiqat H. Improvement of mechanical and biological properties of porous CaSiO₃ scaffolds by poly (D, L-lactic acid) modification. *Acta Biomater*, in press, doi: 10.1016/j.actbio.2007.08.010.
- [17] Kokubo T. Surface chemistry of bioactive glass–ceramics. *J Non-Cryst Solids* 1990;120:138–51.
- [18] Hench LL, Wilson J. Surface-active biomaterials. *Science* 1984;226(4675):630–6.
- [19] Baltag I, Watanabe K, Kusakari H, Taguchi N, Miyakawa O, Kobayashi M, et al. Long-term changes of hydroxyapatite-coated dental implants. *J Biomed Mater Res* 2000;53(1):76–85.
- [20] Brinker C, Sherer G. *Sol–gel Science: the physics and chemistry of sol–gel processing*. San Diego: Academic Press; 1990.
- [21] Chai CS, Gross KA, Ben-Nissan B. Critical ageing of hydroxyapatite sol–gel solutions. *Biomaterials* 1998;19(24):2291–6.
- [22] Ramanan SR, Venkatesh R. A study of hydroxyapatite fibers prepared via sol–gel route. *Mater Lett* 2004;58(26):3320–3.
- [23] Bull SJ, Berasetegui EG. An overview of the potential of quantitative coating adhesion measurement by scratch testing. *Tribol Int* 2006;39(2):99–114.
- [24] Johnson S, Haluska M, Narayan RJ, Snyder RL. In situ annealing of hydroxyapatite thin films. *Mater Sci Eng C* 2006;26(8):1312–6.
- [25] Wei C, Yen J-Y. Effect of film thickness and interlayer on the adhesion strength of diamond like carbon films on different substrates. *Diam Relat Mater* 2007;16(4–7):1325–30.
- [26] Xue W, Liu X, Zheng X, Ding C. Plasma-sprayed diopside coatings for biomedical applications. *Surf Coat Tech* 2004;185(2–3):340–5.
- [27] Wu C, Chang J, Zhai W, Ni S, Wang J. Porous akermanite scaffolds for bone tissue engineering: preparation, characterization, and in vitro studies. *J Biomed Mater Res B Appl Biomater* 2006;78(1):47–55.
- [28] Wu C, Chang J, Wang J, Ni S, Zhai W. Preparation and characteristics of a calcium magnesium silicate (bredigite) bioactive ceramic. *Biomaterials* 2005;26(16):2925–31.
- [29] Wu C, Chang J, Ni S, Wang J. In vitro bioactivity of akermanite ceramics. *J Biomed Mater Res A* 2006;76(1):73–80.
- [30] Liu X, Huang A, Ding C, Chu PK. Bioactivity and cytocompatibility of zirconia (ZrO₂) films fabricated by cathodic arc deposition. *Biomaterials* 2006;27(21):3904–11.
- [31] Pecheva E, Petrov T, Lungu C, Montgomery P, Pramatarova L. Stimulated in vitro bone-like apatite formation by a novel laser processing technique. *Chem Eng J*, in press.
- [32] Vaissieres L, Chaneac C, Tronc E, Jolivet JP. Size tailoring of magnetite particles formed by aqueous precipitation: an example of thermodynamic stability of nanometric oxide particles. *J Colloid Interf Sci* 1998;205(2):205–12.